

Instruments and Methods

Estimation of debris cover and its temporal variation using optical satellite sensor data: a case study in Chenab basin, Himalaya

A. SHUKLA,¹ R.P. GUPTA,¹ M.K. ARORA²

¹*Department of Earth Sciences, Indian Institute of Technology Roorkee, Roorkee, Uttarakhand 247667, India
E-mail: aparna.shukla22@gmail.com*

²*Department of Civil Engineering, Indian Institute of Technology Roorkee, Roorkee, Uttarakhand 247667, India*

ABSTRACT. Debris cover over glaciers greatly affects their rate of ablation and is a sensitive indicator of glacier health. This study focuses on estimation of debris cover over Samudratapu glacier, Chenab basin, Himalaya, using optical remote-sensing data. Remote-sensing image data of IRS-1C LISS-III (September 2001), IRS-P6 AWiFS (September 2004) and Terra ASTER (September 2004) along with Survey of India topographical maps (1963) were used in the study. Supervised classification of topographically corrected reflectance image data was systematically conducted to map six land-cover classes in the glacier terrain: snow, ice, mixed ice and debris, debris, valley rock, and water. An accuracy assessment of the classification was conducted using the ASTER visible/near-infrared data as the reference. The overall accuracies of the glacier-cover maps were found to range from 83.7% to 89.1%, whereas the individual class accuracy of debris-cover mapping was found to range from 82% to 95%. This shows that supervised classification of topographically corrected reflectance data is effective for the extraction of debris cover. In addition, a comparative study of glacier-cover maps generated from remote-sensing data (supervised classification) of September 2001 and September 2004 and Survey of India topographical maps (1963) has highlighted the trends of glacier depletion and recession. The glacier snout receded by about 756 m from 1963 to 2004, and the total glacier area was reduced by 13.7 km² (from 110 km² in 1963). Further, glacier retreat is found to be accompanied by a decrease in mixed ice and debris and a marked increase in debris-cover area. The area covered by valley rock is found to increase, confirming an overall decrease in the glacier area. The results from this study demonstrate the applicability of optical remote-sensing data in monitoring glacier terrain, and particularly mapping debris-cover area.

INTRODUCTION

The lofty Himalaya with snow-clad peaks contain about 5000 glaciers of varying extents, covering an area of approximately 38 000 km² (Kaul, 1999). At global and continental scales, snow with its highly reflective nature and large surface cover has a great impact on regional climate, surface radiation balance and energy exchange and on the utilization of water resources. At regional and local scales and at the level of mountain-valley glaciers, snow cover has an impact on the local climate and the availability of water resources for industry, agriculture, domestic use, etc. (König and others, 2001; Wang and Li, 2003; Kargel and others, 2005). In summer, the annual seasonal snow cover accumulating over the Himalayan glaciers and valleys forms an important source of replenishment for the major perennial river systems of northern India. The mapping and monitoring of snow and glacier characteristics is important for all these reasons (Kargel and others, 2005).

Given the inaccessibility, vastness and harsh climatic conditions of snow/glacier areas, remote sensing appears to be the most appropriate tool for monitoring snow and glacier characteristics (König and others, 2001). Remote-sensing data can be acquired at a range of spectral, spatial and temporal resolutions. Depending on the spectral characteristics of the target to be mapped, remote-sensing data at different resolutions can be selected and various

image-processing operations can be employed to extract the required information. The advent of improved satellite sensors (e.g. Terra ASTER (Advanced Spaceborne Thermal Emission and Reflection Radiometer), Terra MODIS (moderate-resolution imaging spectroradiometer) and Aqua MODIS) has accelerated remote-sensing based glaciological studies.

Remote sensing has varied applications in the field of glaciology, which is evident from a number of studies conducted to extract information from satellite data for specific glaciological tasks (König and others, 2001; Kargel and others, 2005). Extensive studies have been carried out on mapping of snow and glacier cover employing different methods. These include

1. Mapping of glaciers and their retreat via manual digitization of glacier outlines (Hall and others, 1992),
2. Image-ratioing based mapping of various snow and ice types (Hall and others, 1988; Bronge and Bronge, 1999; Paul, 2001),
3. Normalized-difference snow index (NDSI) based snow- and glacier-cover estimation (Dozier, 1989; Hall and others, 1995; Winther and Hall, 1999; Silverio and Jaquet, 2005),
4. Mapping dry and wet snow/ice cover (Gupta and others, 2005),

5. Snow and glacier mapping using image-classification techniques (Aniya and others, 1996; Bronge and Bronge, 1999; Sidjak and Wheate, 1999; Slater and others, 1999),
6. Fractional snow-cover mapping (Rosenthal and Dozier, 1996; Vikhamar and Solberg, 2003; Salomonson and Appel, 2004).

Remote-sensing data acquired from a number of sensors, such as the Landsat Thematic Mapper (TM) and Enhanced TM Plus (ETM+), SPOT (Système Probatoire pour l'Observation de la Terre) Vegetation, the US National Oceanic and Atmospheric Administration (NOAA) Advanced Very High Resolution Radiometer (AVHRR), IRS (Indian Remote-sensing Satellite)-LISS (Linear Imaging Self-Scanning sensor) III and IV, Terra MODIS and Terra ASTER, were used in these studies. Most of the cited works deal with mapping of clean or only marginally contaminated snow/glacier surfaces.

However, many mountain glaciers in the Himalaya, Andes and Alaska ranges and on stratovolcanoes are covered with varying amounts of debris cover. A Himalayan glacier is typically composed of snow; ice; mixed ice and debris (MID); debris; and snowmelt water. Of these, debris cover is one of the most important constituents of a glacier system in controlling snowmelt runoff (Østrem, 1959; Fujii, 1977; Mattson and others, 1993), and the estimation of debris cover is crucial for understanding glacier mass balance (Mattson, 2000; Pelto, 2000). Debris cover near glacier snouts often portends the formation of moraine-dammed lakes, and debris cover over glaciers affects the response of glaciers to climatic changes (Sakai and others, 2000). The changing extent of debris cover is thus considered an important indicator of glacier health (Stokes and others, 2007). In this context, mapping and regular monitoring of debris cover over glaciers from remote-sensing data is highly relevant.

DEBRIS-COVER STUDIES USING REMOTE-SENSING DATA

Most of the glaciers in the Himalaya are covered with varying amounts of debris cover consisting of dust, silt, sand, gravel, cobble and boulders (Nakawo, 1979; Fushimi and others, 1980; Mattson and Gardner, 1989; Rana and others, 1996; Adhikary and others, 2000). Debris cover over glaciers is important for two main reasons:

1. Debris cover on glaciers hinders their mapping and has been recognized as a major problem in glaciological studies (Whalley and others, 1986). The spectral response (i.e. reflectance) of debris cover in the form of digital number (DN) values stored within pixels of digital remote-sensing image data is related to the mixture of reflection from both debris and ice. Ice that is completely covered with debris may not be spectrally distinguishable from adjacent non-glaciated areas. Thus, actual glacier boundaries may be difficult to delineate in regions where they are thickly debris-covered, especially where debris-covered ice abuts talus slopes or old debris (Kääb, 2005).
2. Debris cover has considerable influence on the glacier melting process, so its estimation is considered important for determining glacier runoff and evaluating water resources. Observations of ice ablation under a debris

cover suggest that a very thin debris cover may accelerate melting, while an increasing thickness of debris, particularly in excess of a threshold thickness of approximately 0.02 m, inhibits melting (Østrem, 1959; Loomis, 1970; Fujii, 1977; Mattson and others, 1993). Also, the temporal variation of debris cover over glaciers is correlated with changing regional climate and is hence considered an important indicator of glacier health and local climatic change (Mihalcea and others, 2006; Stokes and others, 2007).

In view of the significance of debris cover in glaciology, various studies with different objectives such as mapping the extent of debris cover and its correlation with glacier recession (Stokes and others, 2007), mapping of different types of supraglacial debris cover (Bishop and others, 1995, 1999) and mapping of debris-covered glaciers (Lougeay, 1974; Bishop and others, 2000, 2001; Taschner and Ranzi, 2002; Paul and others, 2004; Ranzi and others, 2004; Buchroithner and Bolch, 2007; Bolch and others, 2008) were carried out using remote-sensing data. For achieving these objectives, various techniques based on manual delineation (Stokes and others, 2007), multispectral image classification (Bishop and others, 1995, 1999), geomorphometric analysis (Bishop and others, 2000, 2001) or their combinations (Paul and others, 2004), analysis of temperature differences between ice-cored and ice-free debris (Lougeay, 1974; Taschner and Ranzi, 2002; Ranzi and others, 2004) and combinations of geomorphometric parameters and temperature information (Buchroithner and Bolch, 2007; Bolch and others, 2008) have been employed.

These studies indicate that mapping the distribution of glacier debris cover is relevant and that satellite remote sensing offers a powerful tool for this purpose. Although previous works have attempted to map debris-covered glaciers from remote-sensing data, few studies have discussed mapping of the distribution of debris cover over glacier surfaces. In this study, satellite remote-sensing data are used to map debris cover and assess its temporal changes over a glacier in the Chenab basin, Himalaya.

STUDY AREA AND DATA

Study area

The study area of about 200 km² is the catchment and watershed of Samudratapu glacier located in the drainage basin of Chandra river which is a tributary of Chenab river (Fig. 1). It is the second largest glacier in the upper Chandra basin after Bara Shigri glacier. It extends from 32.40° N to 32.55° N and 77.37° E to 77.61° E. The region falls within the Greater Himalaya and constitutes crystalline lithological units throughout. The elevation in the area ranges from 4021 to 6527 m a.s.l. A perspective view of the glacier showing the confluence of the main glacier with its tributary glaciers is shown in Figure 2. The figure shows how the lateral moraines of the two tributary glaciers merge to form the medial moraine of the main glacier at their convergence.

Data

Topographic maps at scale 1 : 50 000, surveyed by Survey of India (SOI) in 1963, were used to georeference the remote-sensing data and to generate a digital elevation model (DEM). Topographic maps were also used to create a mask corresponding to the glacier area.

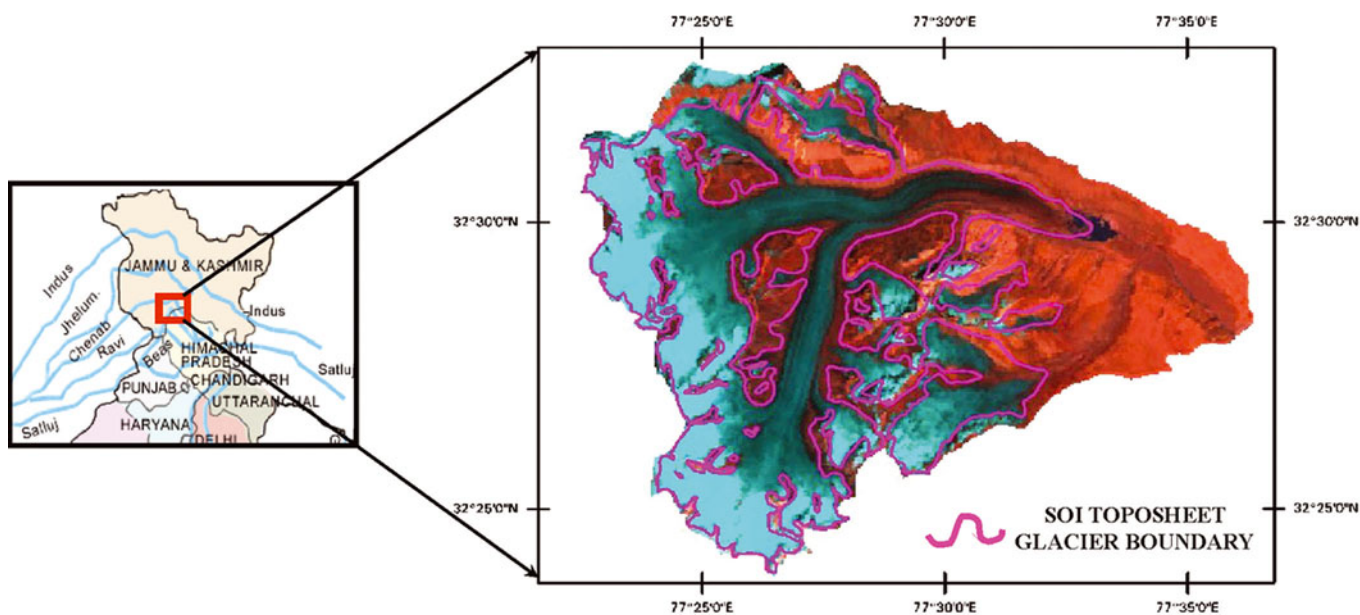


Fig. 1. Samudratapu glacier located in the Chenab basin, Himachal Himalaya. AWiFS image (false-colour composite with band combination, red: B4, green: B3, blue: B2) of the Samudratapu watershed overlaid by the boundary of the glacier digitized from Survey of India topographic maps of 1963.

Remote-sensing data from the IRS-P6 Advanced Wide Field Sensor (AWiFS), IRS-1C LISS-III and the Terra ASTER sensor were used (Table 1). Images for the post-monsoon season (August and September) were selected because during this period the temporary snow cover is at its minimum and all the glacier zones can be clearly demarcated. An ASTER visible/near-infrared (VNIR) image was used as a reference datum for assessing the accuracy of glacier-cover maps, for two reasons: its high spatial resolution (Table 1), and its low temporal difference (1 day) with reference to the AWiFS image. Remote-sensing data from IRS LISS-III and IRS AWiFS provide a temporal difference of 3 years for the study of temporal changes, particularly debris cover. Images from the same month were selected to

eliminate seasonal changes in the areal extents of various classes.

For optimum classification of image objects, it is preferred that the data are expressed in physical units, such as reflectance. As different objects having the same DN values may have differences in spectral reflectance, the use of quantitative spectral reflectance values may improve discrimination between objects. In this work, remote-sensing data have first been converted into topographically corrected reflectance data. Correction of the data for topographic variation requires terrain parameters such as slope and aspect. These input parameters were derived from a DEM created through digitization of contours on SOI topographical maps (scale: 1 : 50 000).

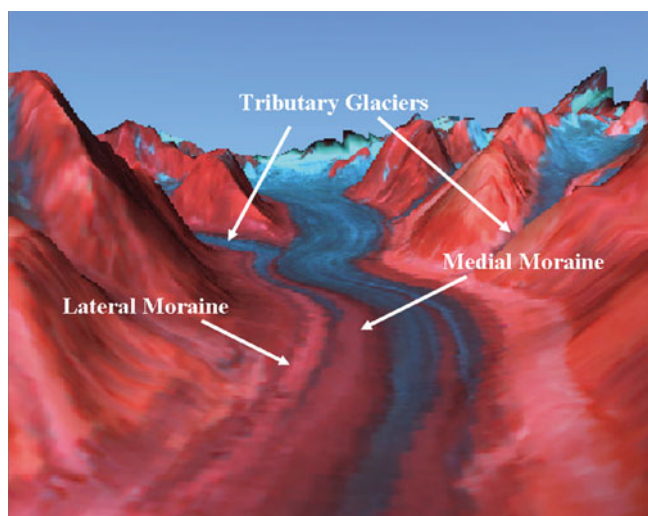


Fig. 2. Perspective view of Samudratapu glacier from Terra ASTER image (false-colour composite with band combination, red: B5, green: B3, blue: B2) draped over a DEM of the area, showing the confluence of tributary glaciers with the main glacier and moraine cover.

METHODOLOGY

The methodology comprises georeferencing of remote-sensing images with topographical maps, computation of topographically corrected reflectance at each pixel of the remote-sensing image and supervised classification of the reflectance data for mapping of six land-cover classes: debris, snow, ice, MID, water, and valley rock. Figure 3 shows the schematic representation of the broad methodology adopted.

Computation of topographically corrected reflectance

Sensors on board various satellites measure the upwelling radiance above the Earth's atmosphere, and represent the received signals as digital numbers, which depend on calibration parameters of the sensor. Radiance reaching the sensor depends upon the target reflectance and the solar irradiance on the target. Reflectance is the ratio of upwelling radiation from the surface to the solar radiation incident on the surface. The magnitude of solar irradiance impinging on a sloping surface greatly depends on the orientation of the target surface. Thus, in a rugged terrain with highly undulating surfaces and steep slopes such as the Himalaya,

Table 1. Specifications of remote-sensing data used in the study

Satellite sensor	Spectral bands	Spatial resolution	Radiometric resolution	Swath width	Date of acquisition	Website
	μm	m		km		
IRS-P6AWiFS	B2: 0.52–0.59 (green) B3: 0.62–0.68 (red) B4: 0.77–0.86 (NIR) B5: 1.55–1.70 (SWIR)	56.0 at nadir and 70.0 at the field edge	10-bit	740.0	7 September 2004	http://www.nrso.gov.in
Terra ASTER (VNIR)	B1: 0.52–0.60 (green) B2: 0.63–0.69 (red) B3: 0.76–0.86 (NIR)	15.0	8-bit	60.0	8 September 2004	http://www.edcdaac.usgs.gov
IRS-1C LISS-III	B2: 0.52–0.59 (green) B3: 0.62–0.68 (red) B4: 0.77–0.86 (NIR) B5: 1.55–1.70 (SWIR)	23.5 23.5 23.5 70.0	7-bit	142.0 142.0 142.0 148.0	13 September 2001	http://www.nrso.gov.in

the reflected radiance reaching the sensor is profoundly influenced by the orientation (slope and aspect) of the target surface. Therefore, for optimum detection/mapping of various target classes, an analysis based on DN values may not be appropriate, since these values inherently include radiometric variations arising from topography, sensor calibration, etc. Hence, the DN values have to be converted into topographically corrected reflectance data.

The variations in remote-sensing reflectance image data due to topography can be adjusted using either of two methods: a method based on image ratioing or a method based on local illumination geometry. The image ratio approach is a simple one, with the assumption that the effect of topography is spectrally uniform and is valid for all incidence angles; however, a major disadvantage of the

method is that the radiometric resolution of the image tends to decrease since ratio images are quite noisy compared to the original data.

The second method is based on illumination modelling and requires a DEM of the area at the same spatial resolution as that of the image, for computing the local incidence angle, *i*. Several methods of topographic correction based on illumination modelling have been developed (e.g. cosine correction, Minnaert correction, statistical–empirical methods, C-correction (Teillet and others, 1982; Teillet, 1986; Meyer and others, 1993)). The bidirectional reflectance distribution function (BRDF) requires definition of surface reflectance characteristics for all possible angle combinations of incidence and reflection, and its use may be the best for topographic correction (Sandmeier and Itten, 1997;

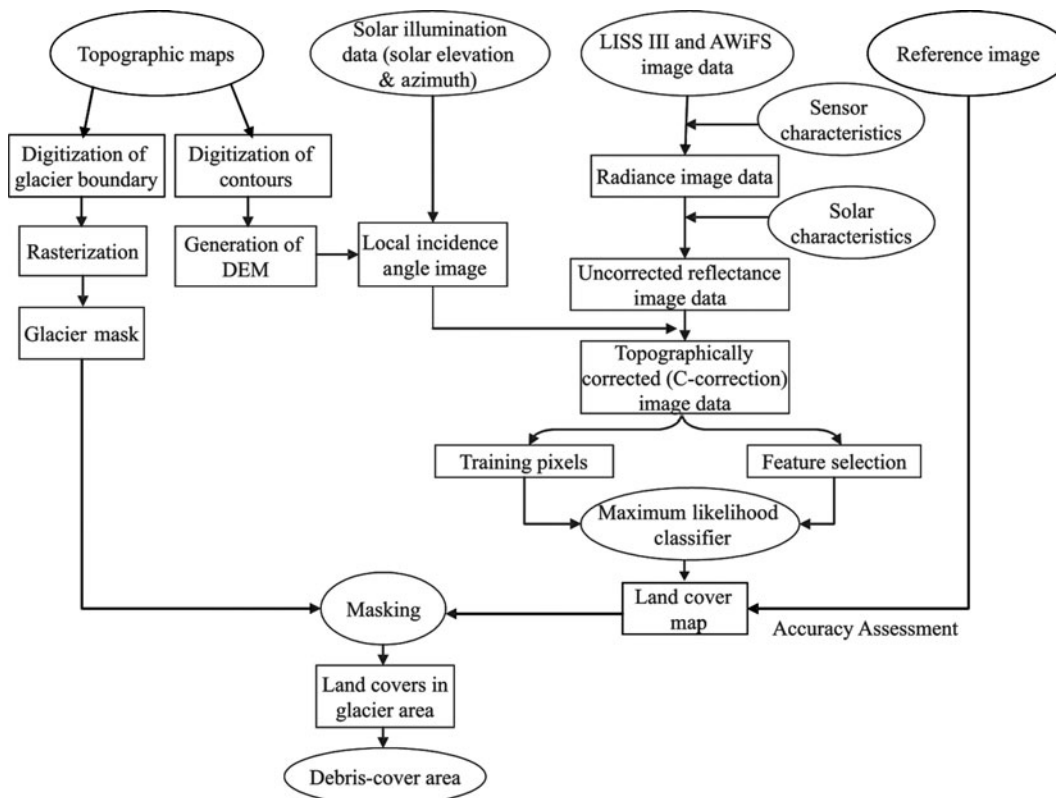


Fig. 3. Schematic data flow of methodology adopted.

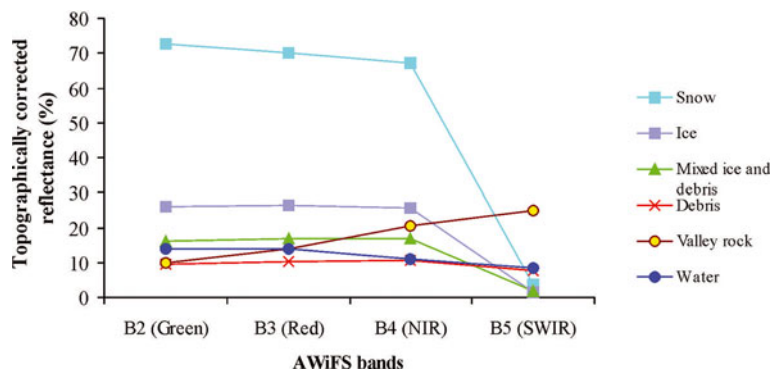


Fig. 4. Typical spectral reflectance curves for the various land-cover classes in the glacier terrain.

Nolin and Dozier, 2000). However, owing to various difficulties in computing the BRDF for field-based problems, more general and approximate approaches are used. Previous studies (e.g. Meyer and others, 1993) indicate that the C-correction method is suitable. It has therefore been used in the present work for topographic normalization. For a detailed description of procedure for C-correction, see Teillet and others (1982), Teillet, (1986), Meyer and others (1993) and Gupta and others (2007).

Supervised classification of reflectance data

The topographically corrected reflectance data were subjected to supervised classification. The aim of digital image classification was to produce thematic maps where each pixel in the image is assigned to a class or a theme on the basis of spectral response at each pixel. There are two basic approaches to digital image classification: supervised or unsupervised (Richards and Jia, 1999). Both have been used widely for snow and glacier mapping (Aniya and others, 1996; Bronge and Bronge, 1999; Sidjak and Wheate, 1999; Slater and others, 1999).

Various standard stages of a supervised image classification have been followed: training, feature selection, allocation and testing (Arora and Foody, 1997). Figure 4

shows the typical reflectance curves of the various land-cover classes of interest. Training areas for all the six classes were selected interactively on the image itself. The total number of training pixels (2631 pixels for the LISS-III image and 915 pixels for the AWiFS image) comprises about 1% of the total number of pixels in the images. Feature selection was performed to quantitatively select that subset of bands (i.e. features) which provides the highest degree of separability between classes to be mapped using transformed divergence (TD) (Mather, 2004). TD is a derivative of simple divergence and its values may range from 0 to 2000 (Jensen, 1996). A TD value of 2000 indicates the highest separability, and values below 1700 indicate low separability.

The separability analysis shows that the three-band combination B2, B4, B5 produces the highest TD values for both AWiFS and LISS-III data. Therefore this band combination was used for classification with a maximum likelihood classifier (MLC). MLC allocates each pixel to the class of which it has the highest probability of membership. Detailed description of this classifier may be found in various works (e.g. Richards and Jia, 1999). The land-cover maps resulting from the MLC are masked with the glacier mask in order to yield glacier-cover maps showing the distribution of the six classes in the glacier area (Fig. 5).

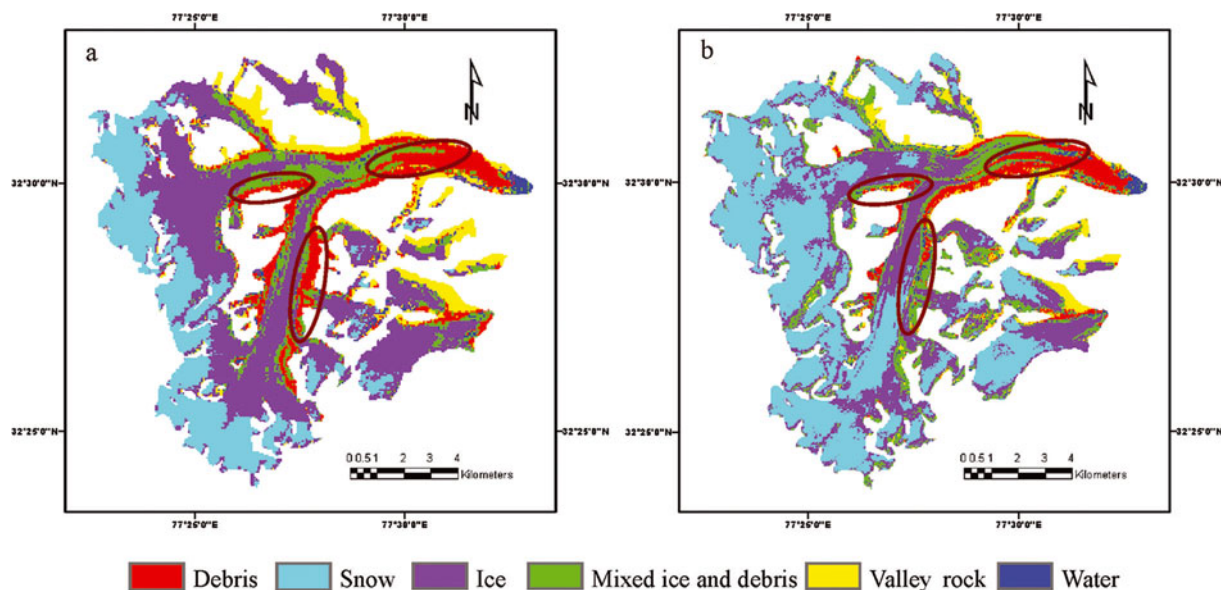


Fig. 5. Glacier-cover maps from (a) AWiFS and (b) LISS-III image data. The brown-coloured ellipses show a marked increase in the debris cover over the glacier from 2001 to 2004 (see text).

Table 2. Producer’s and user’s accuracies (%) (Congalton, 1991) of six land-cover classes in glacier-cover maps derived from AWiFS and LISS-III data of the area

Class	AWiFS image		LISS-III image	
	Producer’s accuracy	User’s accuracy	Producer’s accuracy	User’s accuracy
Snow	88.8	95.0	99.0	99.5
Ice	86.6	71.0	98.4	89.5
MID	78.3	83.0	72.3	94.0
Debris	76.6	82.0	81.9	95.5
Water	91.8	78.0	97.8	65.5
Valley rock	82.3	93.0	95.3	90.5

Classification accuracy assessment

The accuracy of the classified maps was assessed using error-matrix based accuracy measures (Congalton, 1991). An ASTER digital image (VNIR spatial resolution 15 m) was selected as reference data for assessing the accuracy of the image classification. The number of testing pixels collected in equalized random fashion in the case of AWiFS-derived maps is 100 pixels per class. For LISS-III data, it is 200 pixels per class. The error matrix can be utilized to determine the over-all accuracy of the map and individual class accuracies in the form of user’s and producer’s accuracies (Congalton, 1991). The overall accuracy is used to indicate the accuracy of the whole classification (i.e. the number of correctly classified pixels divided by the total number of testing pixels). The producer’s accuracy relates to the probability that a reference sample was correctly mapped, and measures the omission error. The user’s accuracy indicates the probability that a sample from the land-cover map actually matches what it was in the reference data, and measures the commission error.

The error-matrix based accuracy assessment reveals that the methodology applied here has been quite successful in mapping the debris cover and other land-cover classes. Overall accuracies of glacier-cover maps derived from AWiFS and LISS-III data are found to be 83.7% and 89.1% respectively. The relatively high value of overall accuracy for the glacier-cover map obtained from LISS-III image data may be attributed to higher spatial resolution of LISS-III data compared to AWiFS data.

Since the focus of this study is on developing a simple yet effective method for accurate estimation of the debris cover over glaciers, the individual class accuracies have also been examined. The error-matrix based producer’s and user’s accuracy values for all the six classes are given in Table 2. The producer’s and user’s debris-cover accuracy using both the datasets are found to be in the ranges 76–82% and 82–95% respectively. This sufficiently implies that supervised classification of topographically corrected reflectance data is fairly effective for the extraction of debris cover.

However, a careful study and analysis of the error matrix shown in Table 3 reveals that errors of omission and commission are mostly found among four land-cover classes: MID, debris, valley rock, and water. This is largely due to spectral similarity between these classes, which is a major impediment in their precise discrimination. In summary, it can be stated that although the method

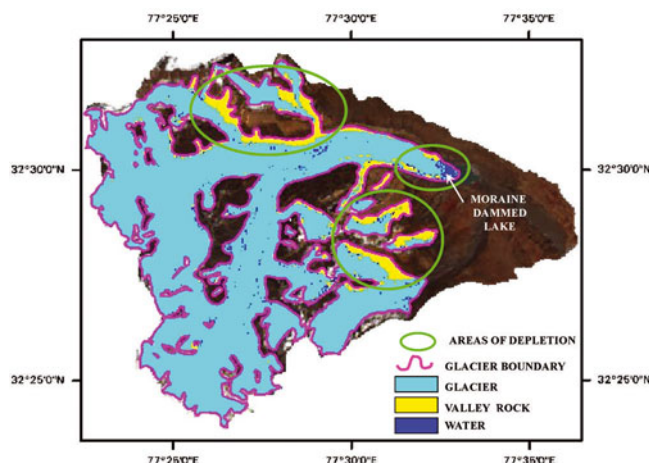


Fig. 6. Comparative assessment of the glacier area obtained from AWiFS (2004) and the glacier boundary derived from SOI toposheets (1963). The false-colour composite (red: B4, green: B3, blue: B2) is from the AWiFS image. All the glacier-cover classes (snow, ice, MID, debris) have been merged into a single class: glacier. Note the presence of valley-rock and water within the glacier area, indicating glacier depletion and recession (circled in green).

proposed here is able to map the debris cover with sufficiently high accuracy, there is scope for further improvement through approaches such as multisource and sub-pixel classification (Srinivasan and Richards, 1990; Arora and Foody, 1997; Binaghi and others, 1997; Arora, 1999; Arora and Mathur, 2001).

CHANGE DETECTION

Deglaciation and recession of the glacier

An intercomparative study of the maps generated from the supervised classification of the remote-sensing data and also the glacier mask created from the SOI toposheets has also been carried out to assess the trends of glacier depletion and recession in the region (Fig. 6).

The presence of valley rock within the glacier area provides evidence of deglaciation and indicates that these areas have been vacated by the glacier, evidently as a result of regional climatic changes. Similarly, the remote-sensing data show the presence of water in the snout region, which actually is a moraine-dammed lake at the terminus of this

Table 3. Error matrix (values in %) for the glacier-cover map produced from AWiFS data

Image classification	Reference data						Row total
	Snow	Ice	MID	Debris	Water	Valley rock	
Snow	95	2	3	0	0	0	100
Ice	12	71	7	4	1	5	100
MID	0	1	83	11	3	2	100
Debris	0	4	7	82	3	4	100
Water	0	2	5	6	78	9	100
Valley rock	0	2	1	4	0	93	100
Column total	107	82	106	107	85	113	600

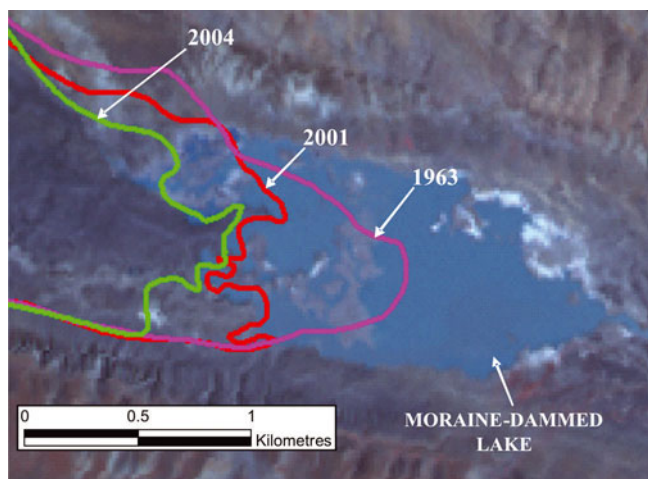


Fig. 7. Change detection of glacier snout. The position of the glacier snout was mapped in 1963 (SOI toposheets), 2001 (IRS-1C LISS-III image) and 2004 (IRS-P6 AWiFS image).

glacier. However, the SOI toposheets (1963) show this area as a part of the glacier. Thus, apparently, due to the recession of the glacier and accompanied melting a moraine-dammed lake has developed at the snout.

The recession and depletion of the glacier has also been estimated quantitatively (Table 4). The glacier area is found to be 110.5 km² in 1963, decreasing to 101.7 km² in 2001, and then further to 96.8 km² by 2004. A detailed study has also been made of the change in glacier snout location (Fig. 7). It is observed that the glacier has receded by 587.7 m (15.5 m a⁻¹) from 1963 to 2001 and by about 168.6 m (56 m a⁻¹) from 2001 to 2004. This is a total retreat of 756.3 m from 1963 to 2004. The increased rate of glacier recession in recent years (2001–04) is considerable and the data conform with the reported accelerated rate of overall glacier depletion (Dobhal and others, 2004; Kulkarni and others, 2005, 2007) and appear to be a result of change in the regional climate.

Temporal variation of debris cover

Intercomparison of the areal estimates of various land-cover classes (debris, snow, ice, MID, water, and valley rock) from the glacier-cover maps obtained from LISS-III (13 September 2001) and AWiFS (7 September 2004) images (Table 5) shows some interesting trends. As stated earlier, remote-

Table 4. Quantitative estimates of glacier depletion for 1976–2001 and 2001–04, from SOI toposheets (1963), LISS-III image (2001) and AWiFS image (2004)

No.	Source	Glacier inventory comparative data		
		Glacier area km ²	Depletion in area km ²	Average rate of glacier depletion km ² a ⁻¹
1.	SOI toposheets (1963)	110.5		
2.	LISS-III data (2001)	101.7	8.8	0.25
3.	AWiFS data(2004)	96.8	4.9	1.63

Table 5. Comparison of the areal estimates of various land-cover classes from classified glacier-cover maps derived from LISS-III and AWiFS data of the area

Land-cover class	Area		Remarks
	LISS-III image (13 Sept. 2001) km ²	AWiFS image (7 Sept. 2004) km ²	
Snow	46.8	25.3	Decrease in snow area
Ice	31.1	45.8	Increase in ice area
MID	16.3	12.5	Decrease in MID area
Debris	7.5	13.3	Increase in debris-cover area
Valley rock	6.0	11.0	Increase in valley-rock area
Water	2.7	2.7	Water area remains almost the same

sensing data from the same month were chosen to minimize the effect of seasonal changes in areal estimates.

The results in Table 5 show that in a span of 3 years (2001–04), the area of debris cover increased by 76.5% from 7.5 km² to 13.3 km². This increase can also be observed clearly in the glacier-cover maps (Fig. 5; areas denoted by brown ellipses). Assessment of such a change in the areal extent of debris cover over glaciers is valuable, as debris cover is not only considered a sensitive indicator of glacier health but also influences the process of glacier melting. Besides debris cover, the areal extents of other classes are also found to vary. The areas of snow cover and MID have decreased, with an accompanying increase in the areas of ice, debris and valley rock. All these changes appear to be intimately linked with the general climatological warming, increased rates of ablation, depletion and recession. Similarly, the MID-covered area has decreased due to melting, leading to an increase in the area covered by debris. Also, the shrinking of the glacier has resulted in an increase in valley rock area. Thus, accelerated rates of recession, overall glacier depletion, and increase in debris cover, as deduced by analysis of remote-sensing data, provide strong evidence of overall degeneration and wasting of the glacier. All these facts again point towards the urgent need for regular monitoring of various glacier land-cover classes, particularly debris cover.

CONCLUDING REMARKS

It is very important to map debris cover over glaciers since it is known to influence the rate of glacier melting to a large extent and is considered an important parameter of glacier health. In this study, supervised classification of topographically corrected optical remote-sensing data (IRS-1C LISS-III and IRS-P6 AWiFS) was carried out in a small part of the Chenab basin. Terra ASTER VNIR data were used as reference data for accuracy assessment. Based on the analysis of results from this study, the following conclusions can be drawn:

1. In this glacier terrain, there are six different land-cover types as characterized by the spectral reflectance data:

snow, ice, MID, debris, valley rock, and water. The separability analysis shows that the band combination B2, B4, B5 has the highest value of transformed divergence for the two remote-sensing images (IRS-1C LISS-III and IRS-P6 AWiFS), indicating maximum separability between the land-cover classes selected.

- Overall accuracies of classification of remote-sensing images via maximum likelihood classification are found to range from 83.7% to 89.1%, whereas the individual accuracy of debris-cover class can be mapped with accuracy ranging from 82% to 95%. This shows that the supervised classification of topographically corrected reflectance data is effective for the extraction of debris cover from remote-sensing data.
- Comparison of the total glacier-cover area obtained from the SOI topographic maps (1963) and the recent satellite remote-sensing data (2001 and 2004) reveals that the glacier area has reduced from 110.5 km² in 1963 to 101.7 km² in 2001, and further to 96.8 km² in 2004. This amounts to an overall deglaciation of 13.7 km² during the past 41 years.
- The glacier snout position was found to have retreated by 587.7 m (15.5 m a⁻¹) from 1963 to 2001 and by about 168.6 m (56 m a⁻¹) from 2001 to 2004. Thus in the past 41 years (1963–2004) the glacier has receded by about 756 m.
- The recent glacier retreat and depletion is found to be accompanied by a marked increase in the extent of debris cover, which has increased by almost 76.5% in a span of just 3 years (from 7.5 km² in 2001 to 13.3 km² in 2004). An increase in valley-rock area is also found during this (2001–04) period.
- Therefore, the accelerated rates of recession and overall glacier depletion observed for the recent years 2001–04, together with the marked increase in debris cover, may be interpreted as strong indicators of the overall degeneration and wasting of the glacier.

The study sufficiently demonstrates the applicability of the remote-sensing data in monitoring glacier terrain, and particularly mapping debris-cover area.

ACKNOWLEDGEMENTS

A. Shukla thanks the Council of Scientific and Industrial Research (CSIR), India, for providing a research fellowship. We thank two reviewers for valuable comments on an earlier version of the manuscript.

REFERENCES

- Adhikary, S., M. Nakawo, K. Seko and B. Shakya. 2000. Dust influence on the melting process of glacier ice: experimental results from Lirung Glacier, Nepal Himalayas. *IAHS Publ.* 264 (Symposium at Seattle 2000 – *Debris-Covered Glaciers*), 43–52.
- Aniya, M., H. Sato, R. Naruse, P. Skvarca and G. Casassa. 1996. The use of satellite and airborne imagery to inventory outlet glaciers of the Southern Patagonia Icefield, South America. *Photogramm. Eng. Remote Sens.*, **62**(12), 1361–1369.
- Arora, M.K. 1999. Thematic information extraction using neural network and fuzzy techniques. *Indian Cartogr.*, **19**, 344–351.
- Arora, M.K. and G.M. Foody. 1997. Log-linear modelling for the evaluation of variables affecting the accuracy of probabilistic, fuzzy and neural network classifications. *Int. J. Remote Sens.*, **18**(4), 785–798.
- Arora, M.K. and S. Mathur. 2001. Multi-source classification using artificial neural networks in a rugged terrain. *Geocarto Int.*, **16**(3), 37–44.
- Binaghi, E., P. Madella, M.G. Montesano and A. Rampini. 1997. Fuzzy contextual classification of multisource remote sensing images. *IEEE Trans. Geosci. Remote Sens.*, **35**(2), 326–340.
- Bishop, M.P., J.F. Shroder, Jr and J.L. Ward. 1995. SPOT multi-spectral analysis for producing supraglacial debris-load estimates for Batura Glacier, Pakistan. *Geocarto Int.*, **10**(4), 81–90.
- Bishop, M.P., J.F. Shroder, Jr and B.L. Hickman. 1999. SPOT panchromatic imagery and neural networks for information extraction in a complex mountain environment. *Geocarto Int.*, **14**(2), 19–28.
- Bishop, M.P., J.S. Kargel, H.H. Kieffer, D.J. MacKinnon, B.H. Raup and J.F. Shroder, Jr. 2000. Remote-sensing science and technology for studying glacier processes in high Asia. *Ann. Glaciol.*, **31**, 164–170.
- Bishop, M.P., R. Bonk, U. Kamp and J.F. Shroder, Jr. 2001. Terrain analysis and data modeling for alpine glacier mapping. *Polar Geogr.*, **25**(3), 182–201.
- Bolch, T., M.F. Buchroithner, A. Kunert and U. Kamp. 2008. Automated delineation of debris-covered glaciers based on ASTER data. In Gomasasca, M.A., ed. *Geoinformation in Europe. Proceedings of the 27th EARSeL Symposium, 4–7 June 2007, Bozen, Italy*. Rotterdam, Millpress, 403–410.
- Bronge, L.B. and C. Bronge. 1999. Ice and snow-type classification in Vestfold Hills, East Antarctica, using Landsat-TM data and ground radiometer measurements. *Int. J. Remote Sens.*, **20**(2), 225–240.
- Buchroithner, M.F. and T. Bolch. 2007. An automated method to delineate the ice extension of the debris-covered glaciers at Mt. Everest based on ASTER imagery. *Grazer Schr. Geogr. Raumforsch.*, **43**, 13–24.
- Congalton, R.G. 1991. A review of assessing the accuracy of classifications of remotely sensed data. *Remote Sens. Environ.*, **37**(1), 35–46.
- Dobhal, D.P., J.G. Gergan and R.J. Thayyen. 2004. Recession and morphogeometrical changes of Dokriani glacier (1962–1995), Garhwal Himalayas, India. *Current Sci.*, **86**(5), 692–696.
- Dozier, J. 1989. Spectral signature of alpine snow cover from the Landsat Thematic Mapper. *Remote Sens. Environ.*, **28**(1), 9–22.
- Fujii, Y. 1977. Field experiment on glacier ablation under a layer of debris cover. *Seppyo, J. Jpn. Soc. Snow Ice*, Special Issue 39, 20–21.
- Fushimi, H., M. Yoshida, O. Watanabe and B.P. Upadhyay. 1980. Distributions and grain sizes of supraglacial debris in the Khumbu glacier, Khumbu region, Nepal. *Seppyo, J. Jpn. Soc. Snow Ice*, Special Issue 41, 18–25.
- Gupta, R.P., U.K. Haritashya and P. Singh. 2005. Mapping dry/wet snow cover in the Indian Himalayas using IRS multispectral imagery. *Remote Sens. Environ.*, **97**(4), 458–469.
- Gupta, R.P., A. Ghosh and U.K. Haritashya. 2007. Empirical relationship between near-IR reflectance of melting seasonal snow and environmental temperature in a Himalayan basin. *Remote Sens. Environ.*, **107**(3), 402–413.
- Hall, D.K., A.T.C. Chang and H. Siddalingaiah. 1988. Reflectances of glaciers as calculated using Landsat-5 Thematic Mapper data. *Remote Sens. Environ.*, **25**(3), 311–321.
- Hall, D.K., R.S. Williams, Jr and K.J. Bayr. 1992. Glacier recession in Iceland and Austria as observed from space. *Eos*, **73**(12), 129, 135, 141.
- Hall, D.K., G.A. Riggs and V.V. Salomonson. 1995. Development of methods for mapping global snow cover using Moderate Resolution Imaging Spectroradiometer (MODIS) data. *Remote Sens. Environ.*, **54**(2), 127–140.
- Jensen, J.R. 1996. *Introductory digital image processing. Second edition*. New York, Prentice Hall.

- Kääb, A. 2005. Combination of SRTM3 and repeat ASTER data for deriving alpine glacier flow velocities in the Bhutan Himalaya. *Remote Sens. Environ.*, **94**(4), 463–474.
- Kargel, J.S. and 16 others. 2005. Multispectral imaging contributions to global land ice measurements from space. *Remote Sens. Environ.*, **99**(1–2), 187–219.
- Kaul, M.K. 1999. *Inventory of the Himalayan glaciers: a contribution to the International Hydrological Programme*. Kolkata, Geological Survey of India. (GSI Special Publication 34.)
- König, M., J.G. Winther and E. Isaksson. 2001. Measuring snow and glacier ice properties from satellite. *Rev. Geophys.*, **39**(1), 1–28.
- Kulkarni, A.V., B.P. Rathore, S. Mahajan and P. Mathur. 2005. Alarming retreat of Parbati glacier, Beas basin, Himachal Pradesh. *Current Sci.*, **88**(11), 1844–1850.
- Kulkarni, A.V. and 6 others. 2007. Glacial retreat in Himalaya using Indian remote sensing satellite data. *Current Sci.*, **92**(1), 69–74.
- Loomis, S.R. 1970. Morphology and ablation processes on glacier ice. *Assoc. Am. Geogr. Proc.*, **2**, 88–92.
- Lougeay, R. 1974. Detection of buried glacial and ground ice with thermal infrared remote sensing. In Santeford, H.S. and J.L. Smith, eds. *Advanced concepts and techniques in the study of snow and ice resources*. Washington, DC, National Academy of Sciences, 487–493.
- Mather, P.M. 2004. *Computer processing of remotely-sensed images: an introduction. Third edition*. Chichester, John Wiley and Sons.
- Mattson, L.E. 2000. The influence of a debris cover on the mid-summer discharge of Dome Glacier, Canadian Rocky Mountains. *IAHS Publ.* 264 (Symposium in Seattle 2000 – *Debris-Covered Glaciers*), 25–33.
- Mattson, L.E. and J.S. Gardner. 1989. Energy exchange and ablation rates on the debris-covered Rakhiot Glacier, Pakistan. *Z. Gletscherkd. Glazialgeol.*, **25**(1), 17–32.
- Mattson, L.E., J.S. Gardner and G.J. Young. 1993. Ablation on debris covered glaciers: an example from the Rakhiot Glacier, Punjab, Himalaya. *IAHS Publ.* 218 (Symposium at Kathmandu 1992 – *Snow and Glacier Hydrology*), 289–296.
- Meyer, P., K.I. Itten, T. Kellenberger, S. Sandmeier and R. Sandmeier. 1993. Radiometric correction of the topographically induced effects on Landsat TM data in an alpine environment. *ISPRS J. Photogramm. Rem. Sens.*, **48**(4), 17–28.
- Mihalcea, D., C. Mayer, G. Diolaiuti, A. Lambrecht, C. Smiraglia and G. Tartari. 2006. Ice ablation and meteorological conditions on the debris-covered area of Baltoro glacier, Karakoram, Pakistan. *Ann. Glaciol.*, **43**, 292–300.
- Nakawo, M. 1979. Supraglacial debris of G2 glacier in Hidden Valley, Mukut Himal, Nepal. *J. Glaciol.*, **22**(87), 273–283.
- Nolin, A.W. and J. Dozier. 2000. A hyperspectral method for remotely sensing the grain size of snow. *Remote Sens. Environ.*, **74**(2), 207–216.
- Østrem, G. 1959. Ice melting under a thin layer of moraine, and the existence of ice cores in moraine ridges. *Geogr. Ann.*, **41**(4), 228–230.
- Paul, F. 2001. Evaluation of different methods for glacier mapping using Landsat TM. *EARSeL eProc.*, **1**(1), 239–245.
- Paul, F., C. Huggel and A. Kääb. 2004. Combining satellite multispectral image data and a digital elevation model for mapping debris-covered glaciers. *Remote Sens. Environ.*, **89**(4), 510–518.
- Pelto, M.S. 2000. Mass balance of adjacent debris-covered and clean glacier ice in the North Cascades, Washington. *IAHS Publ.* 264 (Symposium at Seattle 2000 – *Debris-Covered Glaciers*), 35–42.
- Rana, B., Y. Fukushima, Y. Ageta and M. Nakawo. 1996. Runoff modeling of a river basin with a debris-covered glacier in Langtang Valley, Nepal Himalaya. *Bull. Glacier Res.* **14**, 1–6.
- Ranzi, R., G. Grossi, L. Iacovelli and S. Taschner. 2004. Use of multispectral ASTER images for mapping debris-covered glaciers within the GLIMS project. In *Proceedings of the International Geoscience and Remote Sensing Symposium (IGARSS 2004), 20–24 September 2004, Anchorage, Alaska, USA. Vol. 2*. Piscataway, NJ, Institute of Electrical and Electronic Engineers, 1144–1147.
- Richards, J.A. and X. Jia 1999. *Remote sensing digital image analysis: an introduction. Third edition*. Berlin, etc., Springer-Verlag.
- Rosenthal, W. and J. Dozier. 1996. Automated mapping of montane snow cover at subpixel resolution from the Landsat thematic mapper. *Water Resour. Res.*, **32**(1), 115–130.
- Sakai, A., N. Takeuchi, K. Fujita and M. Nakawo. 2000. Role of supraglacial ponds in the ablation process of a debris-covered glacier in the Nepal. *IAHS Publ.* 264 (Symposium at Seattle 2000 – *Debris-Covered Glaciers*), 119–130.
- Salomonson, V.V. and I. Appel. 2004. Estimating fractional snow-cover from MODIS using the normalised difference snow index. *Remote Sens. Environ.*, **89**, 351–360.
- Sandmeier, S. and K.I. Itten. 1997. A physically-based model to correct atmospheric and illumination effects in optical satellite data of rugged terrain. *IEEE Trans. Geosci. Remote Sens.*, **35**(3), 708–717.
- Sidjak, R.W. and R.D. Wheate. 1999. Glacier mapping of the Illecillewaet icefield, British Columbia, Canada, using Landsat TM and digital elevation data. *Int. J. Remote Sens.*, **20**(2), 273–284.
- Silverio, W. and J.M. Jaquet. 2005. Glacial cover mapping (1987–1996) of the Cordillera Blanca (Peru) using satellite imagery. *Remote Sens. Environ.*, **95**(3), 342–350.
- Slater, M.T., D.R. Slogett, W.G. Rees and A. Steel. 1999. Potential operational multi-satellite sensor mapping of snow cover in maritime sub-polar regions. *Int. J. Remote Sens.*, **20**(15–16), 3019–3030.
- Srinivasan, A. and J. A. Richards. 1990. Knowledge-based techniques for multisource classification. *Int. J. Remote Sens.*, **11**(3), 505–525.
- Stokes, C.R., V. Popovin, A. Aleynikov, S.D. Gurney and M. Shahgedanova. 2007. Recent glacier retreat in the Caucasus Mountains, Russia, and associated increase in supraglacial debris cover and supra-/proglacial lake development. *Ann. Glaciol.*, **46**, 195–203.
- Taschner, S. and R. Ranzi. 2002. Comparing the opportunities of Landsat-TM and ASTER data for monitoring a debris covered glacier in the Italian Alps within the GLIMS project. In *Proceedings of the International Geoscience and Remote Sensing Symposium (IGARSS 2002), 24–28 June, 2002, Anchorage, Alaska, USA. Vol. 2*. Piscataway, NJ, Institute of Electrical and Electronic Engineers, 1044–1046.
- Teillet, P.M. 1986. Image correction for radiometric effects in remote sensing. *Int. J. Remote Sens.*, **7**(12), 1637–1651.
- Teillet, P.M., B. Guindon and D.G. Goodenough. 1982. On the slope-aspect correction of multispectral scanner data. *Can. J. Remote Sens.*, **8**(2), 84–106.
- Vikhamar, D. and R. Solberg. 2003. Snow-cover mapping in forests by constrained linear spectral unmixing of MODIS data. *Remote Sens. Environ.*, **88**(3), 309–323.
- Wang, J. and W. Li. 2003. Comparison of methods of snow cover mapping by analyzing the solar spectrum of satellite remote sensing data in China. *Int. J. Remote Sens.*, **24**(21), 4129–4136.
- Whalley, W.B., H.E. Martin and A.F. Gellatly. 1986. The problem of 'hidden' ice in glacier mapping. *Ann. Glaciol.*, **8**, 181–183.
- Winther, J.G. and D.K. Hall. 1999. Satellite derived snow coverage related to hydropower production in Norway: present and future. *Int. J. Remote Sens.*, **20**(15–16), 2991–3008.